DOI: https://doi.org/10.2138/am-2020-6985

Title: Buoyant Rise of Anorthosite from a Layered Basic Complex Triggered by Rayleigh-Taylor Instability: Insights from a Numerical Modelling Study

Manuscript Number: 6985R2

Authors: Amal Mukherjee, Indian Institute of Technology, Kharagpur, India Subhasish Das, Indian Institute of Technology, Kharagpur, India Dhrubajyoti Sen, Indian Institute of Technology, Kharagpur-721302, India, Bikramjit Bhattacharya, , National Institute of Technology, Durgapur, West Bengal

DOI: https://doi.org/10.2138/am-2020-6985

Revision 3

Buoyant Rise of Anorthosite from a Layered Basic Complex Triggered by Rayleigh-Taylor Instability: Insights from a Numerical Modeling Study

Amal Bikash Mukherjee[1*], Subhasish Das[2], Dhrubajyoti Sen[3], Bikramjit Bhattacharya[4]

[1*] Subodh Park, Bansdroni, Kolkata-700070, India, [2]Department of Geology and Geophysics, Indian Institute of Technology, Kharagpur-721302, India, [3]Department of Civil Engineering, Indian Institute of Technology, Kharagpur-721302, India, [4]Department of Mechanical Engineering , National Institute of Technology, Durgapur, West Bengal – 71320.

[*]Corresponding author: Telephone: 011-91-33-24113139
E-mail: amalbikash@gmail.com

Abstract

A major unsolved problem of the Proterozoic is the genesis and tectonic evolution of the massif type anorthosites. The idea of large scale floating of plagioclase crystals in a basaltic magma chamber eventually generating massif type anorthosite diapirs from the floatation cumulates is not supported by observations of the major layered basic complexes of Proterozoic to Eocene age. In this paper, we test and propose a new genetic process of anorthosite diapirism through Rayleigh-Taylor instability. We have carried out a numerical modeling study of parallel, horizontal, multiple layers of norite and anorthosite, in a model layered basic complex, behaving like Newtonian or non-Newtonian power law fluids in a jelly sandwich model of the continental lithosphere. We have shown that in this pressure-temperature-rheology configuration the model lithosphere generates Rayleigh-Taylor instability, which triggers diapirism of the anorthosite. In our model, the anorthosite diapirs buoyantly rise through stages of simple, symmetrical upwelling and pronounced bulbous growth to a full-blown mushroom-like form. This is the growth path of diapirs in nearly all analog and numerical previous studies on diapirism. Our anorthosite diapirs fully conform to this path. Furthermore, we demonstrate that the progressive diapirism brings in striking *internal* changes within the diapir itself. In the process, the lowermost anorthosite layer rises displacing the upper norite and anorthosite layers as progressively stretched and isolated segments driven to the margin of the rising diapir - a feature commonly seen in natural anorthosite massifs. We propose that a large plume-generated basaltic magma chamber may be ponded at the viscous lower crust or ductile-plastic upper mantle or further down in the weaker mantle of the jelly sandwich type continental lithosphere. The magma may cool and crystallise very slowly and resolve into a thick- layered basic complex with anorthosite layers. Rheologically behaving like Newtonian or non-Newtonian power law fluids, the layers of the basic complex with built-in density inversions would generate RT (Rayleigh-Taylor) instability. The RT instability would trigger buoyant rise of the unstable anorthosite from the layered complex. The upward driven anorthosite, accumulated as anorthosite plutons, would gradually ascend across the lower and middle crust as anorthosite diapirs.

Keywords

Anorthosite, layered complex, Rayleigh-Taylor instability, Diapir

Running Title: Buoyant Rise of Anorthosite

Introduction

Massif-type anorthosites are among the most debated of igneous rocks and constitute a major unresolved puzzle of the Proterozoic geology. Unresolved questions about these rocks relate to their form, structure and tectonic setting, their parental magma and, most importantly, the manner of accumulation of nearly monomineralic (close to 90% or more of An40 – An65 plagioclase) crystalline aggregate from the parental basaltic magma (Bowen, 1917; Emslie, 1985; Ashwal, 1993). More than hundred years ago, Bowen (1917) established the three major plinths of anorthosite research: namely, (1) the anorthosites are not products of the melt of their own composition, (2) the anorthosites are products of fractional crystallization of a gabbroic (basaltic) magma and (3) the sieving off and accumulation of the plagioclase crystals from the parental magma to produce anorthosites was made possible through density-controlled vertical movement of crystals in the magma in a gravity field. Despite differences of opinion regarding the detailed compositional characteristics, a variety of basaltic magma is considered as the parent magma of anorthosites (Bowen, 1917; Emslie, 1985; Longhi and Ashwal, 1985; Ashwal, 1993). A mantle-derived basaltic magma, ponded at the continental Moho, is modeled to undergo extensive fractional crystallization. Plagioclase, one of the crystalline products of this magma, is assumed to rise and collect at the top the magma chamber as floatation cumulates. Being lighter than the lower and middle crustal rocks, the plagioclase rich floatation cumulates would supposedly form distinct massif like bodies and would rise across the lower and middle crusts as diapiric anorthosite intrusions (Longhi and Ashwal, 1985; Ashwal, 1993). Layered basic intrusions are possibly the best instances of a ponded basaltic magma that has undergone fractional crystallization. From detailed investigations of the layered basic intrusions, the cooling and crystallization history, the crystallization dynamics and the overall manner of growth of these intrusions may be obtained (Wager and Brown, 1968; McBirney, 1975; Hunter and Sparks, 1987; McCallum, 1996; Morse et al., 2004; Cawthorn and Ashwal, 2009; Charlier et al., 2015).

Anorthosite layers of varying thickness form an important constituent of nearly all layered basic complexes. The number and thickness of these anorthosite layers vary. There is however no indication of a relationship between the location of the anorthosite layer in the stratigraphic column of the layered complex and its thickness and internal structure, texture and the immediate mafic or ultramafic neighborhood (Ashwal, 1993). In the Stillwater Complex, Montana (Wager and Brown, 1968; Ashwal, 1993; McCallum, 1996) and the Dufec Intrusion, Antarctica (Ford, 1976, 1983; Ashwal, 1993), the anorthosite layers are relatively fewer in number, but make up a substantial portion of the entire complex and are widely separated from one another. In comparison, in the Bushveld Complex of South Africa forty-five anorthosite layers varying in thickness from 1 to 23 m have been reported (Cawthorn and Ashwal, 2009). Notably, the anorthosite layers are not located at the top of any of the major well studied basic complexes, ranging in age from late Precambrian to Eocene - among them the Bushveld Complex (Cawthorn, 2015), Stillwater Complex (McCallum, 1996), Muskox Intrusion (Irvine and Smith, 1967), Dufec Intrusion (Ford, 1976), Skaergaard Intrusion (Nielsen, 2004), the Great Dyke (Schoenberg et al., 2003), and the Kiglapait Intrusion (Morse, 2015). Significantly, the uppermost 100 m of the Bushveld Complex, the largest known layered intrusion, is depleted in plagioclase relative to its cotectic proportions and there is no evidence of floatation or prolonged suspension of plagioclase (Cawthorn and Ashwal 2009, p.1607). Also, we have no evidence of large scale liquid immiscibility operating in the basaltic magma, which can physically separate basic/ultrabasic residual liquids from the floating cumulates of plagioclase crystals in a layered intrusion (Cawthorn and Ashwal, 2009, pp. 1631-1632).

The idea of a large scale plagioclase floatation as cumulates to the top of a basaltic magma chamber and segregation of these cumulates into massif like bodies of anorthosite, eventually invading the lower and middle crust as anorthosite diapirs, does not find support from the large majority of layered intrusions of late Precambrian to Eocene age. Indeed it may well be that large scale floatation and accumulation of plagioclase crystals to the top of the chamber of a cooling basaltic magma building anorthosites did not happen in the Proterozoic.

An effective way of physically separating the plagioclase crystals in the form of magma-soaked crystalline mush from the basaltic magma body is provided by Rayleigh-Taylor (RT) instability. RT instability is a fundamental instability generated at the interface between horizontal layers of fluids of different density in the gravity field, when a fluid of higher density overlies a fluid layer of lower density (Rayleigh, 1883 ; Taylor, 1950; Chandrasekhar, 1981; Ramberg, 1967). In a layered basic complex which has developed parallel horizontal layers of anorthosites within layers of denser rocks e.g., norite, gabbro, dunite, pyroxenite and ore minerals, RT instability will develop at the contact of an anorthosite layer and the layer of a denser rock overlying the anorthosite layer. When the viscosity and the rheology permit treating the rock layers as Newtonian or non-Newtonian power law fluids, the RT instability will generate upward moving protrusions on the layers, which will gradually take the shape of ascending diapirs. It is to be noted here that gravitational segregation may play a major role in the initial formation of the layered basic complex.

In this paper, we present the results of a numerical modeling study, which addresses the possibility of anorthosite diapirism from a layered basic complex triggered by RT instability. We show for the first time that the buoyant force of anorthosite diapirism in a layered basic complex can be treated and understood as generated by gravity and RT instability. We further show that the RT instability disrupts the original anorthosite-norite layered sequence (norite representing the mafic mineral-assemblage in the model layered complex) and sets into motion upward moving protrusions gradually taking the shape of ascending anorthosite diapirs. This is the principal objective of this paper. As the model diapir ascends and evolves into a mushroom-like shape with a pronounced horizontal spread, the individual layers are stretched and separated into arcuate, lensoid bodies, which are displaced towards the border. Some of the anorthosite layers merge and coalesce towards the diapir center and the thinner and more competent norite layers are separated and displaced towards the diapir's margin. For viscosity, density and thickness parameters same as or close to the observed values for all the constituent rocks, the model generates a host of structures that simulate those of a natural anorthosite massif e.g. (1) the overall diapiric structure of the massif with concentric primary layer structures indicating forceful intrusion and (2) the marginally located mafic rock segments of characteristic schlieren like shape, size and geometrical complexities (Balk, 1931, Ashwal, 1993; Mukherjee et al., 1999).

All through this paper, we use the qualification massif-type for anorthosites in the same sense as that of Ashwal (1993), that is, for the well-recognized group of coarse to very coarse grained, plagioclase ($An_{50\,\pm 10}$)-rich, large, commonly domical, igneous rock complexes, generally confined to the middle Proterozoic.

Previous studies

Numerous numerical modeling studies and analog model experiments have shown that RT instability can generate the buoyant force, which enables a diapir or closely analogous structures e.g. a thermal plume to ascend overcoming the resistance of the dense crustal and the mantle overburden (Ramberg, 1967, 1981; Whitehead and Luther, 1975; Talbot, 1977; Jackson and Talbot, 1989; Bittner and Schmeling, 1995; Berovici and Kelly, 1997; Gerya and Yuen, 2003; Molnar and Houseman, 2013; Dutta et al., 2013; Fernandez and Kaus, 2015; Dutta et al., 2016). ;

We briefly discuss the previous studies chronologically in two groups: numerical modeling studies and analog model experiments. Ramberg and coworkers (1981) analytically treated horizontal multilayered crustal rock sequences behaving like Newtonian fluid in the gravity field. They have shown that the density inversions in such sequences spontaneously generate dome-like inflexions that grow into diapirs rising through the superincumbent strata. Growth of diapiric structures beyond the initial stages was studied by finite-element numerical techniques and experimental methods (Berner et al., 1972; Ramberg, 1981). The finite-element investigations showed, in agreement with the analytical fluid dynamics treatment, that the unstable layers evolved from arched domes through pronounced bulbous shapes to full-fledged mushroom like shapes. It was observed that the diapir assumed a mushroom-like shape with lobes hanging around a central core, when the upper surface of the layered sequence was taken to be rigid. With a free and flexible upper surface, the diapir rises more rapidly and the peripheral hanging lobes are absent (Berner et al., 1972, Fig.5). The overall movement pattern of the diapirs does not depend much on the boundary conditions and remains the same. Bittner and Schmeling (1995) made a numerical study of the RT instability at the interface between the granitic crust and the underlying molten basaltic magma at the Moho. The density contrast between the partially molten granite and the overlying solid granite can lead to RT instability resulting in diapiric rise of the partially molten granite. Barnichon et al. (1999) made a finite-element modeling study of a horizontal 4-layer sequence: two granitic layers simulating the upper crust, underlain by a noritic lower crust and at the bottom of the sequence, a relatively low density, low viscosity, buoyant anorthosite layer. Based on different constitutive laws for the different layers, an elastoplastic upper granitic crust and elastic-viscoelastic lower granite, norite and anorthosite layers were considered. But all cases were made essentially Newtonian by assuming a time-dependent viscous behavior obeying a power law with the exponent n = 1. The model of Barnichon et al.(1999) documented rise of an unstable anorthosite layer through the viscous lower crust, beginning as low flexures, changing to bulbous domes and ending up as mushroom-shaped intrusions. Gerya and Yuen (2003) made a 2-D numerical modeling of the RT-instability developed, through hydration and partial melting at the top of a lithospheric slab in a subduction zone. They modeled how diapiric structures, colder than the lithosphere by 300-400^0 C, may form and vertically ascend from this zone. Gorczyk et al. (2012) have shown that RT instabilities may be initiated as a result of heterogeneities in the plastic strength within the lithosphere. The model explains some aspects of the structural and metamorphic events in intra-plate orogeny. Molnar and Houseman (2013) obtained a semi-analytical solution for RT instability of stratified lithosphere consisting of a low density crust over a denser mantle that overlies an inviscid slightly less dense asthenosphere. They showed how the perturbations due to the RT instability cause upwelling or depression of the mantle-lithosphere interface

This is a preprint, the final version is subject to change, of the American Mineralogist (MSA)
Cite as Authors (Year) Title. American Mineralogist, in press.
DOI: https://doi.org/10.2138/am-2020-6985

and affect the free air gravity anomaly at the surface. Fernandez and Kaus (2015) made a 3-D numerical modeling study of down-built salt diapirs initiated by RT instability. Varying the model parameters e.g. initial salt thickness, sedimentation rate, salt viscosity, salt-sediment viscosity ratio and the density of the sediments, they showed that the sedimentation rate has an additional effect on the formation and evolution of 3D-diapir patterns. Dutta et al. (2013) generated RT instability in a model study of horizontal stratified systems simulating a geological setting. The RT instability produced axisymmetric diapirs of varying shapes depending on the density ratio and the influx rate.

Whitehead and Luther (1975) carried out experiments with parallel, horizontal layers of fluids of different density and viscosity. They showed that RT instability, initiated at the interface between a dense layer and an underlying less dense layer, generates evenly distributed vertical wavelike protrusions with nascent plume heads. The amplitude, wave number and rate of growth of these protrusions were variable and depended on the ratio of the density and viscosity of the parallel layers. These protrusions grew with time into mature natural diapir like structures with marginal syncline and necking. Jackson and Talbot (1989) experimentally generated mushroom-shaped diapirs from a set-up of horizontal multilayers with alternately varying density and viscosity and a buoyant layer located lower down in the sequence. They showed that the slower rate of rise of the diapir near the periphery and faster rate near the core produced a toroidal internal circulation within the diapir. This caused extensive stretching, disfigurement and relocation of the layers within the diapir (Jackson and Talbot, 1989, Fig.5c). Dutta et al. (2016) produced diapirs initiated by RT instability in experimental two-layer model systems simulating a geological setting. Investigating the effect of the source layer tilt, they showed that increasing source layer tilt made the diapirs more and more axy-asymmetric. They showed that at source layer tilt higher than 4°, the diapirs become unstable, resulting in a continuous migration of their stems in the up-slope direction. They made a parallel numerical study of these systems providing an understanding of the asymmetric growth of RT instabilities on tilted source layers, which may exist in sedimentary basins and subduction zones.

The above studies assumed an essentially Newtonian behavior of the rocks and the magma of a slow and long cooling history. Plume-lithosphere interaction has been modeled considering the lithosphere as a stagnant viscous lid (Ribe and Christensen, 1994; Doin et al., 1997; Sleep, 1997; Tackley, 2000). A power law behavior of the magma and the wall rock has also been considered by some workers (Weinberg and Podladchikov, 1994, 1995; Miller and Paterson, 1999). Weinberg and Podladchikov (1994) showed that the power law behavior of the country rock ensures a relatively much faster rate of rise of the diapir in the molten state. They also showed that when the magma inside the diapir solidifies progressively from the border to the core, the solidified parts behave like a stiff power law fluid and the diapir may still rise up to a few kilometers, if it remains buoyant. In this study we treat the starting materials, which may be magmatic rocks or magmas or a mixture of both, as both Newtonian and non- Newtonian power law fluids. Details of the fluid models and results are discussed later.

Formulation of the problem

First we formulate the problem in its simplest representation - in terms of two horizontal layers of rocks in a gravity field - a norite layer of higher density overlying the anorthosite layer of lower density (Fig. 1a). If these layers behave like Newtonian fluids or non-Newtonian power law fluids, the flat interface between these layers generates RT instability (Rayleigh, 1883; Taylor, 1950; Chandrasekhar, 1981). An initial perturbation on this interface will set the interface into motion generating wave like upward protrusion of the lower fluid anorthosite into the upper fluid norite. These protrusions will grow exponentially with time in the initial linear regime of the deformation (Oakley 2004) and develop large fold like structures of anorthosite within the norite (Fig. 1b). In this study, we numerically investigate the results of RT instability in generating superposed modes of upward-growing perturbations, when norite and anorthosite occur as a series of multiple, horizontal and parallel layers (Figs. 2a and 2b). We assume the stack of the parallel layers of anorthosite and norite to be simplified versions of a layered basic complex. Our purpose is to understand and to show how the RT instability created between the norite and the anorthosite layers triggers buoyant rise of anorthosite as a diapir.

Methods and assumptions

The numerical modeling study was carried out using the computational fluid dynamics (CFD) software package: FLUENT (Version 6.2) at Indian Institute of Technology, Kharagpur. For the numerical simulations we used the VOF (volume of fluid) method widely used for multiphase flow modeling (Hirt and Nichols, 1982). FLUENT (6.2) uses the finite-volume method to solve the governing equations for the fluid. We have used the two-dimensional double precision solver option in an Eulerian multiphase model, in which all materials were treated in turn as Newtonian and non-Newtonian fluid. This model of FLUENT solves the general conservation equations of mass and momentum adopting a control-volume-based technique, in which the domain is divided into discrete control volumes using a co-processed computational grid. The governing equations in the individual control volumes are integrated, linearized and solved for the updated values of the dependent variables e.g. velocity and pressure. For pressure calculation the Pressure Staggering Option (PRESTO) was used. An unsteady flow formulation obtains the first order, implicit, time-dependent solutions. The method has generated graphic results that are essentially 2D approximations of axysymmetric structures.

For non-Newtonian fluid based modeling, we have used the FLUENT option for pseudoplastic power law fluids. For power law fluids the shear stress $\boldsymbol{\tau}$ is given by

$$\tau = k(\frac{\partial u}{\partial y})^n \text{ .... (1)}$$

Where k is the flow consistency index (SI unit Pa s^n), $\frac{\partial u}{\partial y}$ is the shear rate or the velocity gradient perpendicular to the plane of shear (SI unit s^{-1}) and n is the flow behaviour index. For n=1, the power law fluid becomes the same as Newtonian fluid. For n<1, the power law fluid is called pseudoplastic power law fluid.

The FLUENT code has been validated by a wide range of fluid dynamic studies of multiphase flow (Sobieski, 2009; Subhas, et al., 2012; Ganapathy, et al., 2013; Lukes and Haake, 2014). Flow behaviour of large scale geological structures e.g. mantle plumes and diapirs have been numerically modeled using FLUENT (Dutta, et al., 2013; Dutta, et al., 2014, Dutta, et al., 2016). Dutta (Dutta, et al., 2016) in particular have used the FLUENT code in a numerical modeling study of diapir growth on tilted source layers triggered by R-T instability. An important part of this study was a set of parallel physical experiments generating RT instability and diapiric growth on tilted source layers. By comparing the diapir growth parameters of the FLUENT-supported numerical study and the growth parameters in the physical experiments, Dutta et al. (2016) were able to reach an excellent validation of the FLUENT code for geological studies.

The solution-adaptive mesh refinement feature of FLUENT allows the user to refine or coarsen the mesh based on geometric and numerical solutions. For numerical computation we have adopted mixed mesh sizing and mixed resolution for each image. Initially we surveyed the modelled areas at low numerical resolution and determined areas where low, high or very high resolutions were necessary. In image areas where there are greater details like layer boundaries, layer mixing, layer separation etc we have used finer mesh size and higher resolution. In a dynamic grid we have used the square grid varying from 100m x 100m to 10km x 10km with the average grid size being 1km x 1km. In the scale of our diapir images (Figs.3, 4, 5, 6, 7, 8), an approximately 1mm x 1 mm image area is clearly resolved by 200 m x 200 m resolution (200 m x 200 m square grid) employed in the computation. Therefore the relatively small structural details in the scale of a few hundred meters e.g. separated layers, stringers and enclaves in our diapir models (Figs. 4, 5, 7, 8) represent real physical objects and not numerical artifacts.

For the simulation study, we have adopted a 42 km thick model crust of nearly identical properties as that assumed by Barnichon et al. (1999). Two variants of the model have been analyzed. They differ only in the number and thickness of alternate anorthosite and norite layers in the lower part of the crust. The physical and geometrical parameters of the constituent rock layers are given in Tables 1 and 2. Diagrammatic vertical cross sections of the two variants of the model are shown in Fig. 2a (four layer model) and Fig. 2b (six layer model). The upper 15 km of the model crust is granitic, having a density of 2770 kg/m^3 and a dynamic viscosity of 3.5 x 10^{20} Pa s. It is divided into a 13 km thick upper granite layer UG and a 2 km thick lower granite layer LG. UG is taken to be a rigid solid and not incorporated in the calculations, while LG along with all anorthosite and norite layers in the 29 km thick lower crust have been treated by FLUENT as viscous, incompressible Newtonian fluid and as pseudoplastic power law fluid. The lower crust differs from Barnichon's model in that it is an ensemble of 4 or 6 alternate layers of anorthosite and norite. In the first variant (Fig. 2a), a 21 km thick upper norite layer overlies a 3-layer sequence of anorthosite (1 km) - norite (1 km) - anorthosite (4 km). In the second variant (Fig. 2b), a 19 km thick upper norite layer overlies a 5-layer sequence of anorthosite (1 km) - norite (1 km) - anorthosite (1 km) - norite (1 km) - anorthosite (4 km). The total thickness of the model crust is 42 km in both variants and the assumed density and viscosity values are the same as those adopted by Barnichon et al. (1999), except for the lowermost anorthosite layer, for which a lower value of dynamic viscosity 1.8 x 10^{18} Pa s has been adopted. The density values are well within the range accepted by Hall (1986) and https://gpg.geosci.xyz. The rheologial profile was computed (Barnichon et al., 1999) using viscosity parameters, which were retrieved using the power law values of Carter and Tsenn (1987) and the method of Davy and Cobold (1991, We have used the parameters of Barnichon et al. (1999) keeping in mind our intent of comparing our results with those of Barnichon et al. (1999). An order of magnitude lower dynamic viscosity value for the lowermost anorthosite layer is assumed to be reasonable, because temperature, the factor strongly influencing viscosity, would most probably be significantly higher at the bottom of the model crust. As a boundary condition, the upper surface of the model crust has been taken to be free and flexible. We have adopted a no-slip boundary condition for the vertical walls and the bottom boundary. The 13 km thick upper granite (UG) has been assumed to be solid and excluded from the calculation. So, a corresponding overburden pressure, P, due to UG on the underlying layered sequence was calculated as $P = \rho . g . h$, where ρ, g, and h represent density, acceleration due to gravity and overburden thickness respectively. This is taken as an approximation since the buoyancy stresses are expected to be small and are ignored. Since we have adopted a free and flexible upper surface, UG would be free to accommodate a vertical movement in response to the calculated deformation of the layers lower down in the column. P was set as the operating pressure condition in FLUENT. The initial perturbation of the lowermost anorthosite-norite contact at the axis of symmetry was taken as sinusoidal with amplitude of 500 m. Smaller initial perturbation generates similar structures at longer simulation time. In a comparable study (Dutta et al., 2016, p.1819) initial perturbations from 0.1 to 0.5 times the source layer thickness did not cause any qualitative variations in the diapir geometry, though the simulation run time varied. Other interlayer contact surfaces were initially horizontal.

Results

4-layer Model (Newtonian)

Progressive diapirism is confined to the 4-layer anorthosite-norite complex under the granite cover and is shown by the two-dimensional axisymmetric approximation in Fig 5. There are two stages of the diapiric growth. In the first stage, there is a significant upward growth of a domical structure (Fig. 3). An interesting feature of this stage is that inside the structure there is significant breaching and merging of layers. A magnified view of the domical structure shows the breaching of the norite layer and merging of the anorthosite layers more clearly (Fig, 4). Fig. 5 shows advanced stage of diapirism. The central upwelling has grown into a mushroom shaped diapir with the top showing a hint of a hanging lobe all around. The mushroom shaped diapir head has detached itself from the layered sequence below and has moved up with a trail hanging down. The fold in the 4-layered sequence below and the clear point of breach from where the diapir tore itself from its source and went up mark a critical stage in the progressive diapirism, when the buoyant force has torn apart and lifted the diapir head and a straggling tail apart from the base (Fig. 5). There are strong geometrical similarities between the numerically generated diapiric growth stages presented here and the RT-triggered diapiric growth stages reported from the analogue experiments of Dutta et al. (2016 Figs. 3, 4, 5,). The well developed mushroom-like structure of the diapir with a hint of a peripheral hanging lobe all round (Fig.5) is comparable to the results of Berner et al. (1972), Jackson and Talbot (1989) and Barnichon et al. (1999).

6-layer Model (Newtonian)

The progressive diapirism is confined within the 6-layer anorthosite-norite group and is shown by two-dimensional axisymmetric approximations in Figs. 6, 7, 8. The granite cover has remained undisturbed except for a gentle warp at the base. The stages of growth and deformation of the diapir in the 6-layer model are broadly similar to the same in the 4-layer model. The diapir growth begins with a strong upward arching of the layers into a domical structure (Fig, 6). Here the lowermost anorthosite layer has ascended upwards, breached the overlying norite layer and coalesced with an upper anorthosite layer. In the next stage (Fig. 7) the central dome has moved further up as a bulbous structure showing pronounced changes in the internal geometry of the norite and anorthosite layers. Extensive breaching, tearing apart and coalescence of layers mark this stage. The most prominent result of this internal deformation is that the lowermost anorthosite layer has intruded upwards, completely breached the top of the central dome, merged with parts of the upper two anorthosite layers and has formed an extended, centrally located funnel-shaped intrusive body (Fig. 7). The two breached norite and two breached anorthosite layers have been peripherally displaced and pushed down (Fig. 7). A horizontal section across the axisymmetric funnel-shaped body (Fig. 7), about halfway between the top and the base would show a central, circular anorthosite intrusive body surrounded by concentric, partly complete or

DOI: https://doi.org/10.2138/am-2020-6985

incomplete rings of norite and anorthosite. Natural anorthosite diapirs of approximately similar outcrop pattern are known.

In the following stage, the diapir head has moved further up and has evolved into a flattened mushroom-like shape with pronounced peripheral curling (Fig. 8). The diapir is now detached from its root-like source and is trailed by a narrow cylindrical stem hanging down from the centre. The internal geometry of the diapir head is now more complicated. The most significant change is that the thick, spread out shield-like top of the diapir is now almost entirely made up of anorthosite. All along its circular margin, separated and deformed segments of norite and anorthosite have curled up and taken position under the shield-like anorthosite overhead. On the whole, there is now an apparent segregation of anorthosite and norite into separate bodies, with anorthosite overlying norite. A noteworthy feature of the 6-layer model is the strong growth of satellite diapirs (Figs. 7, 8). A pair of diapiric upwellings, equidistant from the centrally located main diapir and slightly tilted symmetrically towards it, have developed and evolved initially following more or less the same pattern as the main diapir.

Non Newtonian models

We have made runs of the 4-layered and the 6-layered models, treating the material as a pseudoplastic power law fluid. The overall patterns of deformation in the Newtonian and the non-Newtonian models are similar. The structure of the 4-layer non-Newtonian model at a moderately advanced stage of deformation is shown in Fig. 9 and the same of the 6-layered model at a similar stage is shown in Fig. 10. A strong diapiric growth is evident in the non-Newtonian models also. The non-Newtonian diapirs grow from an arched up dome to a flattened mushroom-like structure. The characteristic internal changes within the diapir head e.g. gradual ascent and coalescence of the anorthosite layers forming an extended thick centrally located uniformly anorthositic shield can be seen in the non-Newtonian models also. For both 4-layer and 6-layer non-Newtonian power law models power law exponent 0.6 has been used (Tables 1 and 2).

Discussion

Reviewing the numerical results

Our numerical results show that anorthosite diapirs may buoyantly rise in response to RT instability from a horizontal, *multilayered* norite-anorthosite complex with built-in density inversions and Newtonian or power law non-Newtonian rheology. In both of our 4-layer and 6-layer models, the pattern of diapirism remains the same and records an overall similarity with the results of the previous workers, except that our experiment on *multilayered* norite-anorthosite models is the first experiment connecting anorthosite diapirism with RT instability. The external form changes from a simple symmetrical upwelling through a bulbous protrusion to a well-developed mushroom-like shape with a pronounced horizontal spread. This is the classical growth path of progressive diapirism of gravity driven horizontal layers, as has been repeatedly demonstrated by analog and numerical experiments carried out by previous workers (Berner et al., 1972; Ramberg, 1981, Figs 7.31, 7.32; Jackson and Talbot, 1989; Talbot at al., 1991; Barnichon et al., 1999, Figs. 9, 10; Dutta et al., 2013; Dutta et al., 2016, Figs. 3, 5).

Our models have generated internal geometrical changes of layer splitting, layer coalescence and layer dispersal towards the border. The ascending lower layers of the complex progressively push up, pierce, break apart and displace the upper layers towards the margin of the rising diapir front, ultimately driving parts of the displaced layers down the side of the diapir. This has led to inversion of the original layer sequence. This has resulted in coalescence of the anorthosite segments towards the domical center and dispersal of the norite segments towards the border. .

The small discrete structures crowded near the border of the diapir top resemble the small volumes of dark coloured mafic rocks e.g. norite, gabbronorite, monzonorite, ferrodiorite, ferrogabbro, and jotunite commonly occur at or near the margin of anorthosite massifs (Ashwal 1993). Generally medium grained and layered, these rocks occur as extended bands or short lenticular bodies grading to sub-meter sized schlieren, which are concordant with the primary layer structures of the anorthosite pluton (Balk, 1931; Buddington, 1939; Anderson, 1966; Emsley, 1980; Owens et al., 1993). We have already mentioned that a horizontal section halfway across the axisymmetric funnel-shaped body of our 6-layer diapir in an advanced stage of growth (Figs.7, 8) would resemble the outcrop of a central, circular or nearly circular anorthosite pluton surrounded by concentric, partly complete or incomplete arcuate rings of basic rock and anorthosite segments.

Lithosphere rheology and RT induced anorthosite diapirism The crucial condition needed for RT induced anorthosite diapirism to operate is that both the norite layers (representing mafic and ultramafic layers) and the anorthosite layers behave like Newtonian or power law non- Newtonian fluids. In our numerical modeling study, we have made the *assumption* that the norite and anorthosite layers in the experiment conditions behave like Newtonian and power law non-Newtonian fluids. Actually the real earth rheology provides support to this assumption.

For rheology of the lithosphere, we adopt the density structure of the lithosphere and the upper mantle after Turcotte and Schubert (2002) and Burov and Guillou-Frottier (2005). Realistically, the continental lithosphere has been treated as a multilayered structure of varying long term (>1 myr) strength. In this multilayered lithosphere (called the jelly sandwich lithosphere) a weak viscous lower crust is sandwiched between a strong brittle-elastic upper crust and a ductile-plastic upper mantle (Burov and Diament, 1995; Burov and Watts, 2006; Burov and Guillou-Frottier, 2005). A different rheological model of the continental lithosphere (called the crème-brûleé lithosphere) has been proposed by Jackson (2002) in which the strength of the crust is confined to the uppermost brittle layer and the mantle is weak. In a generalized discussion of the continental lithosphere models, all models with a weak mantle have been grouped under the crème-brûlée type and all models with a weak lower crust have been grouped under the jelly sandwich type (Burov and Watts, 2006, p. 4; Fig. 6, p. 8). Burov and Watts (2006) have argued that the crème brûlée model is not acceptable because it is unable to explain either the persistence of mountain ranges or the integrity of the downgoing slab in collisional systems.

An illustration of the jelly sandwich lithosphere (of short term mechanical ithosphere thickness of 80 km) may have about a 20 km thick brittle-elastic upper crust (E), an about 20 km thick viscous lower crust (V) and about a 40 km thick ductile plastic upper mantle (P) (Burov and Watts, Fig. 1 C, 2006). In numerical experiments on the plume head- continental lithosphere interactions using a realistic EVP formulation of the layered lithosphere (Burov and Guillou-Frottier, 2005), the effective viscosity at the base of the lithosphere was taken to be between 10^{19} and 5×10^{19} Pa s . This range matches the post-glacial rebound data (Turcotte and Schubert, 2002) for continental lithosphere. The data of 90 years of the post-1906 San Francisco earthquake analysed by Kennar and Segall (2003) are consistent with the deep lower crustal or mantle layer viscosity of $\geq 9.5 \times 10^{19}$ Pa s.

In this study, we prefer the jelly sandwich model to the crème brûlée model of the lithosphere rheology (Jackson, 2002), because this model represents a *group* of layered continental lithosphere models (Burov and Watts, 2006, p. 4) and can account for the wide range of T_e (effective elastic thickness of the lithosphere) values observed due to the wide variation in composition, geothermal gradient, and crustal thickness in continental lithosphere (Burov and Diament, 1995).

A large volume of cooling basaltic magma ponded in a relatively old and steady state section of the lithosphere would still share a Newtonian or power law non-Newtonian rheology with the lithosphere. Indeed the viscosity of the cooling basaltic magma would be considerably lower than the viscosity of the lithosphere section where the magma body is ponded. Experimentally determined viscosity of two pyroxene melt compositions ($MgSiO_3$ and $CaSiO_3$) decreases with pressure, initially at a very fast rate and then at a slower rate (Cochain et al., 2017).The comparison of this data with previous results, obtained from molten Fe_2SiO_4 (Spice et al., 2015), molten $CaMgSi_2O_6$ (Reid et al., 2003) and molten peridotite (Liebske et al., 2005), shows a convergence of their viscosity values at 13 GPa toward 20 – 30 mPa s. In contrast, the viscosity range at the base of the jelly sandwich lithosphere is between 10^{19} and 5 x 10^{19} Pa s (Burov and Guillou-Frottier , 2005). This enormous difference in the rheology of the lithosphere and the cooling magma ponded in it should exist for a very long period of time, given that the ponded magma may cool and crystallize extremely slowly. The rheology of the cooling basaltic magma is therefore likely to remain well within the bounds of Newtonian and non-Newtonian power law rheology for a very long time and would remain competent to generate RT instability.

Model anorthosite diapirs and natural anorthosite diapirs

We briefly address here some of the most prominent similarities between model anorthosite diapirism and the dynamics of natural anorthosite diapirs. Model anorthosites ascend from the layered complex as isolated diapirs. Natural anorthosites typically occur as isolated intrusions in the middle and lower crust (Ashwal 1993), often showing clear evidence of forceful diapiric intrusion . During the ascent of the model diapirs, the anorthosite and the subordinate mafics are *relocated* within the diapir – the anorthosite is concentrated more to the centre of the diapir top and the mafics more to the border. Most natural anorthosite massifs have closely associated small volumes of mafic rocks e.g. norite, gabbronorite, leuconorite, ferrodiorite, ferrogabbro and jotunite commonly occurring at or near the margin of the massif (Balk, 1931; Buddington 1939; Emslie, 1980; Owens et al. 1993; Ashwal, 1993; Wiebe, 1990).

The model diapir retains its domical shape during the ascent. Natural diapirs preserve the domical structure with evidence of diapiric intrusion. Parallelly oriented magmatic flow layers making a circular pattern of rotating dip and strike directions and symmetrically oriented primary joints e.g cross joints, longitudinal joints and diagonal joints are abundantly developed in natural diapirs. The diapir-aureole contact zones preserve the diapiric signatures e.g. close to border parallelism of planar structures and increase of strain intensity towards the border. The Banpur-Balugaon and Bolangir anorthosite massifs are mid-crustal (5-6 kbar, 600-700^0 C) anorthosite diapirs of the Eastern Ghats, India (Mukherjee et al.1999). The remarkable unity and symmetry of the magmatic flow structures and the primary fracture structures of these two anorthosite diapirs, statistically proved by stereographic projections of a large field data base, illustrate a real, buoyant, en bloc , upward movement of the diapirs through pronounced stretching and flow on circularly striking sets of parallel planes and by ductile bulk shortening at the border (Mukherjee et al, 1999).

The Mattawa anorthosite massif of the Grenville Province, Quebec is a small (about 15 km diameter) subcircular dome, has magmatic foliations (steep at the border and gentle at the centre) and is concentrically zoned by successive intrusions of compositionally different anorthosites (Anderson, 1969; Owens and Dymek, 2011). The massif is identified as a diapiric intrusion (Owens and Dymek, 2011)

Conclusions

The continental lithosphere from the lower crust downwards into the mantle behaves like a Newtonian or power law non- Newtonian fluid (Burov and Diament, 1995; Burov and Watts, 2006; Burov and Guillou-Frottier, 2005) . So, a layered basic intrusion, located in the continental lithosphere, would also behave like a Newtonian or power law non-Newtonian fluid and all horizontal contact interfaces between anorthosite and an *overlying* denser rock in the layered complex would generate RT instability. We believe, a strong probability exists that RT instability, in the presence of necessary conditions in the continental lithosphere, would run its full course as a normal hydrodynamic process and would trigger ascent of the unstable anorthosite from the layered basic complex as anorthosite diapir.

This conclusion reached from general arguments alone gets a strong support from our numerical modeling study presented in this paper. We have shown in this study that RT instability may indeed trigger progressive diapirism of anorthosite in a horizontal multilayered basic complex in the jelly sandwich model of continental lithosphere. Thus RT instability has been shown to provide anorthosite diapirism with a testable dynamic basis. We have shown that the model anorthosite diapirs change their external and internal structures as they ascend. The full-fledged diapirs gradually evolve from a bulbous protrusion to a mushroom shaped form with hanging peripheral lids. This is the classical growth path of nearly all analog and numerically modeled diapirs in the literature and our model anorthosite diapirs fully conform to this. Internally, the buoyant force of diapirism stretch and pierce the successive layers of anorthosite and norite, partially relocate these layers by coalescing the anorthosite into an extended, centrally located domical top and pushing the norite layers towards the border. A horizontal section halfway across a fully evolved diapir would show a circular or sub-circular pattern of partly continuous arcuate separations of norite and subordinate anorthosite near the diapir border – a feature observed in natural anorthosite plutons. The model anorthosite diapirs share with natural anorthosite diapirs common features e.g. isolated domical intrusions, layered structures near the border bearing imprints of forceful intrusion and closely associated small volumes of assorted basic rocks and anorthosite near the border.

In current research, one of the preferred modes of origin of the basaltic magma parental to a layered basic complex is through mantle plume magmatism (Scarrow, J., H., Cox, K., G., 1995; Spandler, et al., 2005; Polyakov, et al., 2009; Owen-Smith et al., 2017). A plausible scenario of msassif anorthosite genesis and diapirism may be outlined as follows. A plume-generated large basaltic magma chamber located at the viscous lower crust, ductile-plastic upper mantle, or further down in the weaker upper mantle of a jelly sandwich lithosphere may cool extremely slowly, crystallize and fractionate at the same time and resolve into a layered basic complex with thick layers of anorthosite with layers of basic and ultrabasic rocks and ore minerals. Behaving like Newtonian or non-Newtonian power law fluids, the layered basic complex, with built-in density inversions, would generate RT instability and trigger upward motion of the unstable anorthosite layers.The upward driven anorthosite, assembled as anorthosite plutons, would gradually ascend across the lower and middle crust as anorthosite diapirs.

Implications

The most important implication of this paper is that it provides a dynamic basis and a testable hypothesis for the diapiric rise and intrusion of massif type anorthosite from the earth's mantle into the crust. The role of Rayleigh-Taylor instability in explaining the buoyant rise of anorthosite from a layered basic complex is equally valid for small and medium size diapirs like those of the Eastern Ghats (Banpur-Bolangir, Balugaon, Mukherjee et al. 1999) and the Grenville Province (Mattawa,Labrieville, Owens and Dymek, 2001, 2005), or also for very large anorthosite massifs like the 17000 km ^{2} Lac St Jean of the Canadian Grenville (Woussen et al. 1981), and the 15000 km ^{2} Kunene anorthosite massif, Namibia (Menge, 1998). This validity depends on one precondition, namely, that there is one or more density inversions in a horizontal stack of rocks e.g. norite, gabbro, ultramafic rocks, ore minerals and anorthosite in the gravity field, all these rocks behaving like Newtonian or non-Newtonian power law fluids. This dependence is unrelated to the size of the parent magmatic body.

Acknowledgment

This paper has benefited from the reviews by three anonymous reviewers. We thank all of them.

References

Anderson, A., T., Jr. (1969) Mineralogy of the Labraville Anorthosite, Quebec. American Mineralogist 51, 1671- 1711.

Ashwal, L., D. (1993) Anorthosites. Springer Verlag, Berlin, 422 pp.

Balk, R. (1931) Structural Geology of the Adirondack anorthosite. Mineralogische und Petrographische Mitteilungen 41, 308-434.

Barnichon, J., D., Havenith, H., Hoffer, B., Charlier, R., Jongmans, D., and Duchesne, J. C., (1999) The deformation of the Egersund- Ogna anorthosite massif, south Norway: finite- element Modelling of diapirism. Tectonophysics 303, 109 -130

Berner, H., Ramberg, H., and Stephansson, O. (1972) Diapirism in theory and experiment. Tectonophysics 15, 197-218.

Bercovici, D., and Kelly, A. (1997) The non-linear initiation of diapirs and plume heads. Physics of The Earth and Planetary Interiors 101, 119-130.

Bittner, D., and Schmeling, H. (1995) Numerical Modelling of Melting Processes and Induced Diapirism in the Lower Crust. Geophysical Journal International 123, 59-70.

Bowen, N., L. (1917) The Problem of the Anorthosites. Journal of Geology 25, 209 – 243.

Buddington, A., F. (1939) Adirondack igneous rock and their metamorphism. Geological Society of America Memoir 7, 343 pp.

Burov, E., B., and Diament, M. (1995) The effective elastic thickness (T_e) of continental lithosphere: What does it really mean? Journal of Geophysical Research 100, 390- 3927

Burov, E., B., and Guillou-Frottier, L. (2005) The plume head- continental lithosphere interaction using a tectonically realistic formulation of the lithosphere. Geophysical Journal International 161, 469-490

Burov, E. B., and Watts, A. (2006) The long-term strength of continental lithosphere: “jelly sandwich” or “crème brûlée”? GSA Today 16, 4- 10.

Carter, N., L.,and Tsenn, M. (1987) Flow properties of continental lithosphere.Tectonophysics136, 27- 63.

Cawthorn, R., G. (2015) The Bushveld Complex, South Africa. 2015. Layered Intrusion. In: Charlier, B., Namur, O., Latypov, R., and Tegner, C.(Eds Layered Intrusions. Springer, Dordrecht, 517-587.

Cawthorn, R., G., and Ashwal, L., D. (2009) Origin of Anorthosite and Magnetitite Layers In the Bushveld Complex, Constrained by Major Element Compositions of Plagioclase. Journal of Petrology 50, 1607-1637.

Chandrashekhar, S. (1981) Hydrodynamic and Hydromagnetic stability. Dover Publications, INC. New York, 653 pp.

Charlier, B., Namur, O., Latypov, R.,and Tegner, C.(Eds) (2015) Layered Intrusions. Springer Netherlands, 748 pp.

Cochain, C., Sanloup, C., Leroy, C., and Kono, Y. (2017) Viscosity of mafic magmas at high pressures.Geophysical Research Letters, 44t, 818- 826.

Davy, P., and Cobbold, P., R. (1991) Experiments on shortening of a 4-layer Lithosphere. Tectonophysics 188, 1- 25.

Doin, M., P., Fleitout, L., and Christensen, U. (1997) Mantle convection and stability of depleted and undepleted continental lithosphere. Journal of Geophysical Research 102. 2771 -2787.

Dutta, U., Sarkar, S.,and Mandal, N. (2013) Ballooning versus curling of mantle plumes: views from numerical models. Current Science 104. 893-903.

Dutta, U., Sarkar, S., Baruah, A.,and Mandal, N. (2014) Ascent modes of jets and plumes in a stationary fluid of contrasting viscosity. International Journal of Multiphase Flow 63. 1- 10.

Dutta, U., Baruah, A.,and Mandal, N.(2016) Role of source-layer tilts in the axi-asymmetric growth of diapirs triggered by a Rayleigh-Taylor instability. Geophysical Journal International. 206, 1814-1830.

Emsley, R., F. (1980) Geology and Petrology of the Harp Lake Complex, Central Labrador: an example of Elsonian magmatism. Geological Survey of Canada Bulletin 293.136 pp.

Emsley, R., F. (1985) Proterozoic anorthosite massifs. In: Tobi, A., C., Touret, J., L., R., (Eds) The Deep Proterozoic Crust in the North Atlantic Provinces. Nato Advanced Study Institute Reidel, Dordrecht, 39-60

Fernandez, N., and Kaus, B., J., P. (2015) Pattern formation in 3-D numerical models of down-built diapirs initiated by Rayleigh-Taylor instability. Geophysical Journal International 202. 1253- 1270.

Ford, A., B. (1976) Stratigraphy of the Layered Gabbroic Dufe Intrusion, Antarctica. U. S. Geological Survey Bulletin 1405 – D, 36 p.

Ford, A., B. (1983) The Dufec Intrusion Antarctica and a survey of its minor metals and possible resources. In Petroleum and Mineral Resources of Antarctica. (Ed. Behrendt, J., C.,) US Geological Survey Circular 909.

Ganapathy, H., Shooshtari, A., K.,and Ohadi, M. (2013) Volume of fluid-based numerical modeling of condensation heat transfer and fluid flow characteristics in microchannels. International Journal of Heat and Mass Transfer 65. 62-72.

Gerya, T., V., and Yuen, D., A. (2003) Characteristics- based marker- in-cell method with conservative time-differences scheme for modeling geological flows with strongly variable transport properties. Physics of the Earth and Planetary Interiors 140. 293-318.

Gorczyk, W., Hobbs, B.,and Gerya, T. (2012) Initiation of Rayleigh-Taylor instabilities in intra- cratonic settings. Tectonophysics 514- 17, 146-155

Hall, J. (1986) The physical properties of layered rocks in deep continental crust. In: Dawson, J., B., Carswell, D., A., Hall, J., Wedepohl, K., H., (Eds).The Nature of the Lower Continental Crust. Geological Society of London Special Publication 24, 51-62.

Hirt, C., W.,and Nichols, B., D. (1982) Volume of fluid (VOF) method for the dynamics of free boundaries. Journal of Computational Physics 39. 201-225.

https://gpg.geosci.xyz 2017, GeoSci Developers.

Hunter, R., H.,and Sparks, R., S., J. (1987) The Differentiation of the Skaergaard intrusion. Contribution to Mineralogy and Petrology 95, 451-461.

Irvine, T., N.,and Smith, C., H. (1967) The ultramafic rocks of the Muskox intrusion. In Ultramafic and Related Rocks (ed Wyllie P.J.), 38-49. Wiley.

Jackson, M., P., A.,and Talbot, C., J. (1989) Anatomy of mushroom- shaped diapirs. Journal of Structural Geology 11, 211-230.

Jackson, J. (2002) Strength of the continental lithosphere: Time to abandon the jelly sandwich? GSA Today 12, 4-10

Kenner, S., J., and Segall, P. (2003) Lower crustal structure in northern California: Implications from strain-rate variations following the 1906 San Francisco earthquake. Journal of Geophysical Research 108 (B11996. 2011,\ doi: 10, 1029- 20

Liebske, C., Schmickler, B., Terasaki, H., Poe, B., Suzuki, A., Funakoshi, K., Ando, R.,and Rubie, D. (2005) Viscosity of peridotite liquid up to 13 GPa: Implications for magma ocean viscosities. Earth and Planetary Science Letters 240, 589- 604.

Longhi, J., and Ashwal L., D (1985) Two-Stage Models for Lunar and Terrestrial Anorthosites: Petrogenesis without a Magma Ocean, Journal of Geophysical Research 90. C571- C584.

Lukes, R., A.,and Haake, S., J.(2014) A CFD Analysis of Flow around a Disc. Procedia Engineering 72, 685-690.

McBirney, A., R. (1975) Differentiation of the Skaergaard Intrusion. Nature 253, 691-694.

McCallum, I., S. (1996) The Stillwater Complex: A review of the Geology. In: Cawthorn R, G. (ed.), Layered Intrusions, Amsterdam, Elsevier Science, 441-48.

Menge G. F. W. (1998) The antiformal structure and general aspects of the Kunene Complex, Namibia. Zeitschrift derDeutschenGeologische Gesellschaft 149/3, 431-448.

Miller, R., B.,and Paterson, S., R. (1999) In defense of magmatic diapirs. Journal of Structural Geology 21, 1161-1173.

Molnar, P.,and Houseman., A.(2013) Rayleigh- Taylor instability lithospheric dynamics, and gravity anomalies. Journal of Geophysical Research 118, 2544-2557

Morse, S., A., Brady, J., B.,and Sporledar, B., A. (2004) Experimental petrology of the Kiglapait intrusion: Cotectic trace for the Lower Zone at 5kb in graphite. Journal of Petrology 45, 2225-2259

Morse, S., A. (2015) Kiglapait Intrusion, Labrador. In Charlier, B., Namur, O., Latypov, and R., Tegner, C. (Eds.) layered Intrusions, Springer-Dordrecht, 589-648.

Mukherjee A., Jana P., and Das S. (1999) The Banpur- Balugaon and Bolangir anorthosite diapirs of the Eastern Ghats, India: Implications for the msassif anorthosite problem. International Geology Review 41(3), 206-242.

Oakley,J. (2004) Rayleigh-Taylor Instability Notes. 9 pp.

Owens B. E.,and Dymek, R. F. (2001) Petrogenesis of the Labrieville Alkalic Anorthosite Massif, Grenville Province, Quebec. Journal of Petrology 42, 1519-1546.

Owens, B. E.,and Dymek, R. F. (2011) Rediscovery of the Mattawa Anorthosite Massif, Grenville Province, Quebec. Canadian Journal of Earth Sciences 42(10), 1699-1718.

Owens, B., E., Rockow, M., W., Icenhower, J., P., and Dymek, R., F. (1993) Jotunites from the Grenville Province, Quebec: petrological characteristics and implications for massif anorthosite genesis. Lithos 30, 57-80

Owen-Smith, T., M., Ashwal, L., D., Sudo, M., and Trumbull, R., B. (2017) Age and Petrogenesis of the Doros Complex, Namibia, and Implications for early Plume-derived melts in the Parana-Etendeka LIP. Journal of Petrology 58, 423-442

Polyakov, G., V., Shelepaev, R., A., Hoa, T., T., Izokh, A., E., Balykin, P., A., Phuong, N., T, .Hung, T., Q.,and Nien, B., A. (2009) The Nui Chua layered peridotite-gabbro complex as manifestation of Permo-Triassic mantle plume in northern Vietnam. Russian Geology and Geophysics 50, 501-516.

Ramberg, H. (1967) Model Experimentation of the Effect of Gravity on Tectonic Processes. Geophysical Journal International 14. 307-329.

Ramberg, H. (1981) Gravity, Deformation and the Earth's Crust in Theory, Experiments and Geological Application. (2^{n} edn.).Academic Press, London. 452 pp.

Rayleigh, Lord (John William Strutt) (1883) Investigation of the character of the equilibrium of an incompressible heavy fluid of variable density. Proceedings of the London Mathematical Society 14.170-177.

Reid, J., Suzuki, A.,Funakoshi, K., Terasaki, H., Poe, B., Rubie, D.,and Ohtani, E. (2003) The viscosity of CaMg Si_2O_6 liquid at pressures up to 13 GPa, Physics of Earth and Planetary Interior 139,45-54.

Ribe, N., M.,and Christensen U. R. (1994) 3- Dimensional modeling of plume-lithosphere interaction. Journal of Geophysical Research Atmospheres 99, 669-682

Scarrow, J., H., and Cox, K., G. (1995) Basalts Generated by Decompressive Adiabatic Melting of a Mantle Plume: a case study from the Isle of Skye, NW Scotland. Journal of Petrology 36, 3-22.

Schoenberg, R., Nägler, Th., F., Gnos, E., Kramers, J., D.,and Kamber, B., S. (2003) The Source of the Great Dyke, Zimbabwe and Its Tectonic Significance. The Journal of Geology 111, 565- 578

Sobieski, W. (2009) Momentum Exchange In Solid - Fluid System Modeling with Eulerian Multiphase Model. Drying Technology. An International Journal 27, 653-671.

Spandler, C., Mavrogenes, J.,and Arculus, R. (2005) Origin of chromitites in layered intrusions: Evidence from chromite- hosted melt inclusions from the Stillwater complex. Geology 33, 893 - 896.

Spice, H., C., Sanloupe, B., Cochain, B., de Grouchy, C.,and Kono, Y. (2015) Viscosity of liquid fayalite up to 9 GPa. Geochimica Cosmochimica Acta 148, 219- 227.

Subhas, S., Saji, V., F., Ramakrishna, S.,and Das, H., N. (2012) CFD Analysis of a Propeller Flow and Cavitation. International Journal of Computer Applications. 55, 26-33.

Tackley, P., J. (2000) Mantle convection and plate tectonics: toward an integrated physical and chemical theory. Science 288, 2002-2007.

Talbot, C., J. (1977) Inclined and asymmetric Upward-moving gravity structures. Tectonophysics 42, 159-181.

Talbot, C.,J., Ronnlund, P., Schmeling, H., Koyi, H.,and Jackson, M., P., A. (1991) Diapiric spoke patterns.Tectonophysics 188, 187-201.

Taylor, G., I. (1950) The instability of liquid perpendicular to their planes. Proceedings o the Royal Society of London. Series A, /Mathematical and Physical Sciences 201, 192- 196.

Turcotte, D., L.,and Schubert, G. (2002) Geodynamics (Second Edition). Cambridge University Press. 863 pp.

Wager, L., R.,and Brown, G., M. (1968) Layered Igneous Rocks. Oliver and Boyd. 588 pp.

Weinberg, R., F.,and Podladchikov, Y. (1994) Diapiric ascent of magmas through power law crust and mantle. Journal of Geophysical Research: Solid Earth. 99, 9543-9559.

Weinberg, R., F.,and Podladchikov, Y., Y. (1995) The rise of solid- state diapirs. Journal of Structural Geology 17, 1183-1195. Whitehead, J., A., Jr., and

Luther, D., S. (1975) Dynamics of laboratory diapir and plume models. Journal of Geophysical Research 80, 707-717

Woussen, G., Dimroth, E., Corriveau, L. ,and Archer, P. (1981) Crystallization and emplacement of the Lac St-Jean anorthosite massif (Quebec, Canada). Contributions to Mineralogy and Petrology 76, 343- 350.

List of Illustrations

Fig. 1(a) *Parallel horizontal layers of norite and anorthosite in the gravity field.* Norite (yellow) of higher density overlies anorthosite (pink).

Fig. 1(b) *The folds in the anorthosite and norite layers developed at the anorthosite –norite interface in response to R-T instability.*

Fig. 2 (a) *The 4-layer norite (yellow)-anorthosite (pink) model topped by the lower and upper granite (white) layers.*

Fig. 2 (b) *The 6-layer norite (yellow)-anorthosite (pink) model topped by the lower and upper granite (white) layers*.

Fig. 3 *Beginning of diapirism in the 4-layer model in the form of a gentle, symmetrical upwelling of the anorthosite and norite layers.*

Fig. 4 *A magnified view of the top of the nascent diapir (Fig 3).* Details of the upward growth of the domical structure are shown. The norite layer has breached. The lower anorthosite layer has moved up pushing apart the broken norite layer and has merged with the top anorthosite layer.

Fig 5 *Growth of the 4-layer diapir*. The nascent diapir has moved up and grown into a domical top with the lobe hanging all around. The diapir head has detached itself from the layered sequence below and has moved up with a trail hanging down. The sharp angled fold in the layered sequence below and the clear point of breach from where the diapir tore itself preserve details of the pull-tear-lift action of the vertically directed buoyant force generated by RT instability.

Fig. 6 *The 6-layer nascent diapir*. Two norite layers have breached and moved apart. The room vacated by the norite layers has been occupied by three anorthosite layers which have coalesced at the top.

Fig 7 *Advanced stage of growth of the 6-layer model*. The diapir has grown into a bulbous structure. The layers have been progressively stretched, breached, pierced and and separated into small segments. The lower anorthosite layers have occupied the top of the diapir, pushing away the sepsarated norite layers towards the border. A central wide-topped anorthosite dome with a few scattered isolated norite segments has formed.

Fig 8 *Fully developed mushroom structure developed from the 6- layer model*. The mushroom head is flattened and at the top the lobes are hanging all around and curled inwards. The norite has been completely pushed out of the diapir head to a hollow cup-like structure beneath the diapir head. The separation of norite and anorthosite in the diapir head is nearly complete. The anorthosite at the top has formed an extended domical structure and resembles a domical anorthosite intrusive. The diapir head has been detached from the base with a trail hanging downwards. The top anorthosite later has been drawn and pulled upwards by the buoyant force up to a point where the diapir head has been torn apart and has moved upwards with a hanging tail. At the base of the lower granite and on top of the diapir head a gentle warp has formed. A pair of satellite diapirs have formed on both sides of the centrally located main diapir.

Fig 9. *Moderately advanced stage of non-Newtonian deformation of the 4-layer model*.

Fig 10. *Moderately advanced stage of non-Newtonian deformation of the 6-layer model.*

DOI: https://doi.org/10.2138/am-2020-6985

Table 1: Parameters used for the 4-layer model

Material	Thickness (km)	Density (Kg/m^3)	Viscosity (Pa s)	Type
Upper Granite	13	2700	3.5×10^{20}	Brittle solid
Lower Granite	2	2700	3.5×10^{20}	Newtonian/ Power law fluid
Norite	21	3000	6.8×10^{19}	Newtonian/ Power law fluid
Anorthosite	1	2750	1.8×10^{19}	Newtonian/ Power law fluid
Norite	1	3000	6.8×10^{19}	Newtonian/ Power Law fluid
Anorthosite	4	2750	1.8×10^{18}	Newtonian/ Power law fluid
Power law exponent	0.6			

Table 2: Parameters used for the 6-layer model

Material	Thickness (km)	Density (kg/m^3)	Viscosity (Pa s)	Type
Upper Granite	13	2700	3.5×10^{20}	Brittle solid
Lower Granite	2	2700	3.5×10^{20}	Newtonian/ Power law fluid
Norite	19	3000	6.8×10^{19}	Newtonian/ Power law fluid
Anorthosite	1	2750	1.8×10^{19}	Newtonian/ Power law fluid
Norite	1	3000	6.8×10^{19}	Newtonian/ Power law fluid
Anorthosite	1	2750	1.8×10^{19}	Newtonian/ Power law fluid
Norite	1	3000	6.8×10^{19}	Newtonian/ Power law fluid
Anorthosite	4	2750	1.8×10^{18}	Newtonian/ Power law fluid
Power law exponent	0.6			

This is a preprint, the final version is subject to change, of the American Mineralogist (MSA)
Cite as Authors (Year) Title. American Mineralogist, in press.
DOI: https://doi.org/10.2138/am-2020-6985

Table 1: Parameters used for the 4-layer model

Material	Thickness (km)	Density (Kg/m^3)	Viscosity (Pa s)	Type
Upper Granite	13	2700	3.5×10^{20}	Brittle solid
Lower Granite	2	2700	3.5×10^{20}	Newtonian/ Power law fluid
Norite	21	3000	6.8×10^{19}	Newtonian/ Power law fluid
Anorthosite	1	2750	1.8×10^{19}	Newtonian/ Power law fluid
Norite	1	3000	6.8×10^{19}	Newtonian/ Power Law fluid
Anorthosite	4	2750	1.8×10^{18}	Newtonian/ Power law fluid
Power law exponent	0.6			

This is a preprint, the final version is subject to change, of the American Mineralogist (MSA)
Cite as Authors (Year) Title. American Mineralogist, in press.
DOI: https://doi.org/10.2138/am-2020-6985

Table 2: Parameters used for the 6-layer model

Material	Thickness (km)	Density (kg/m^3)	Viscosity (Pa s)	Type
Upper Granite	13	2700	3.5×10^{20}	Brittle solid
Lower Granite	2	2700	3.5×10^{20}	Newtonian/ Power law fluid
Norite	19	3000	6.8×10^{19}	Newtonian/ Power law fluid
Anorthosite	1	2750	1.8×10^{19}	Newtonian/ Power law fluid
Norite	1	3000	6.8×10^{19}	Newtonian/ Power law fluid
Anorthosite	1	2750	1.8×10^{19}	Newtonian/ Power law fluid
Norite	1	3000	6.8×10^{19}	Newtonian/ Power law fluid
Anorthosite	4	2750	1.8×10^{18}	Newtonian/ Power law fluid
Power law exponent	0.6			

(a)

(b)

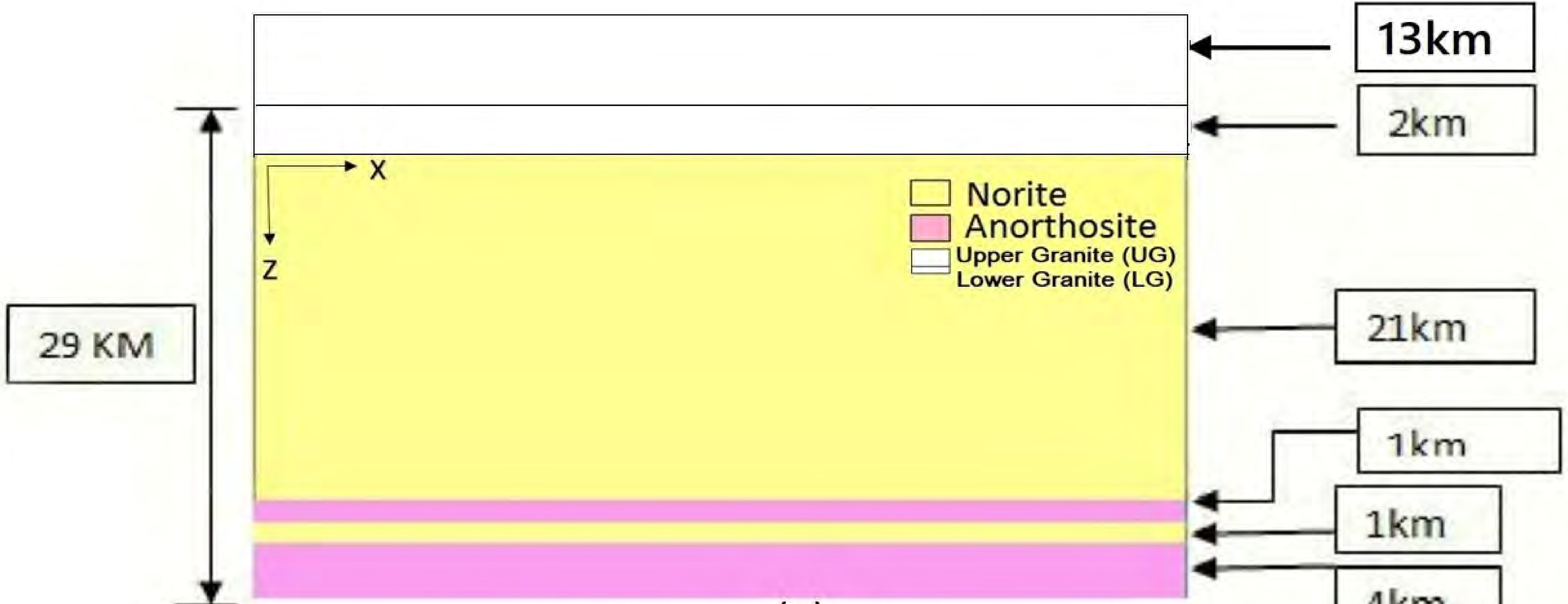
13km
2km
X
Z
Norite
Anorthosite
Upper Granite (UG)
Lower Granite (LG)
29 KM
21km
1km
1km
4km

(a)

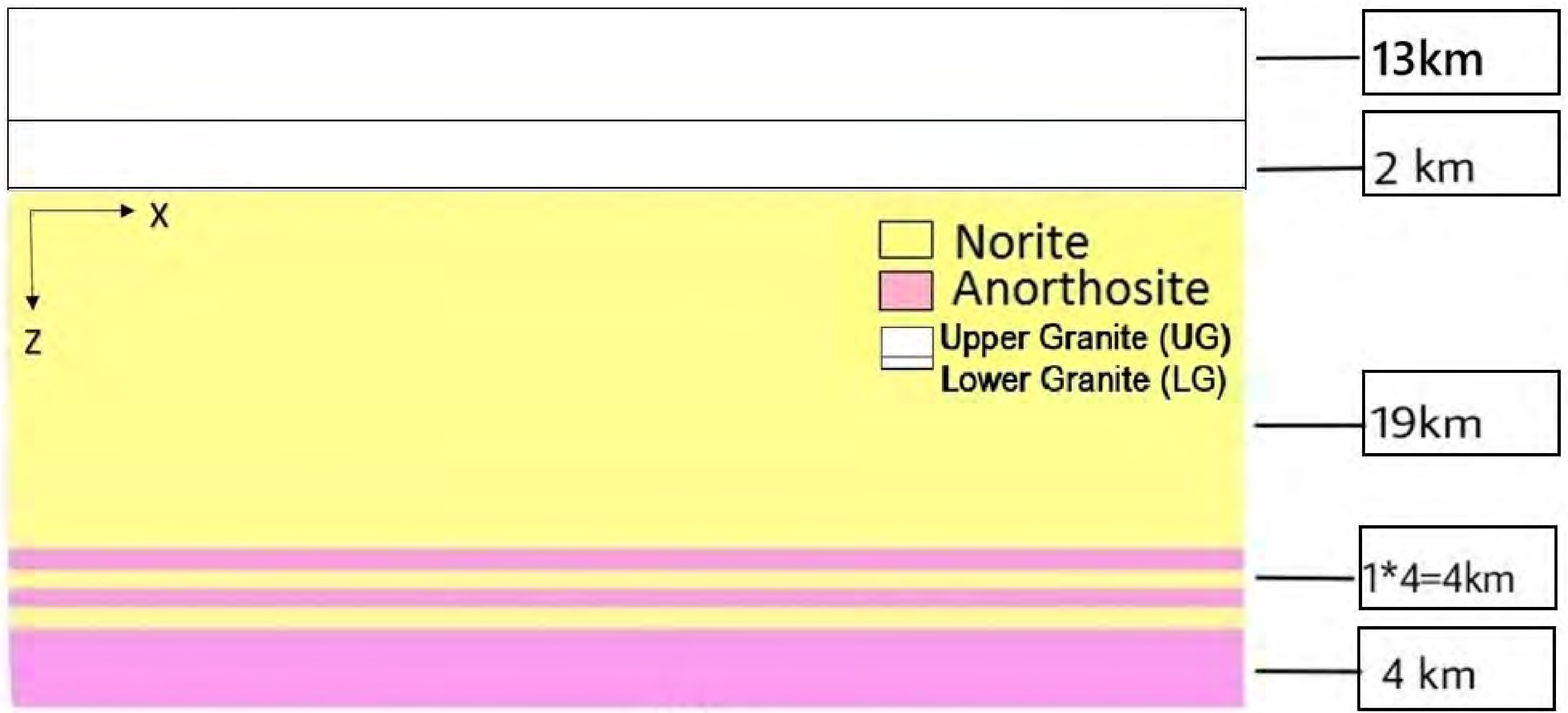
13km
2 km
X
Z
Norite
Anorthosite
Upper Granite (UG)
Lower Granite (LG)
19km
1*4=4km
4 km

(b)

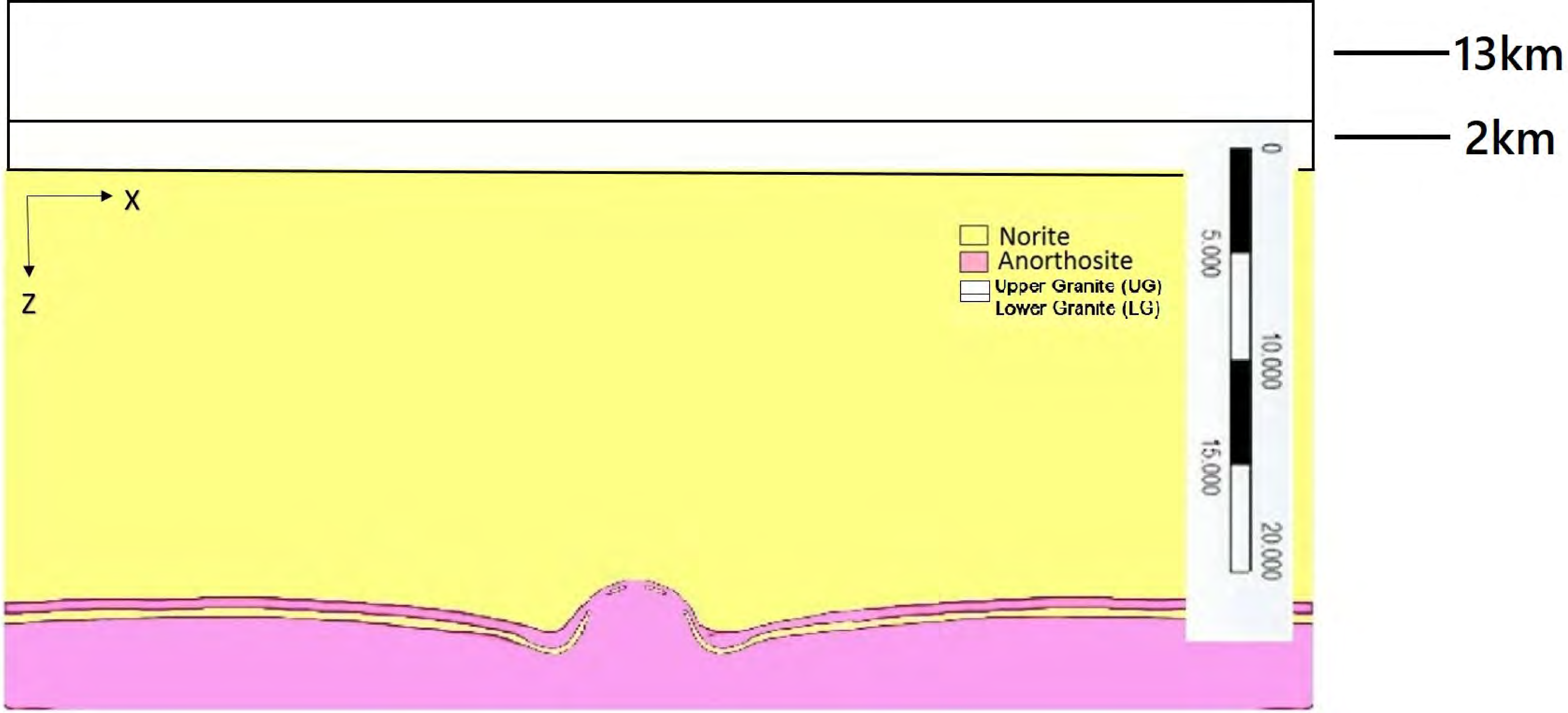
13km
2km
X
Z
Norite
Anorthosite
Upper Granite (UG)
Lower Granite (LG)
0
5.000
10.000
15.000
20.000

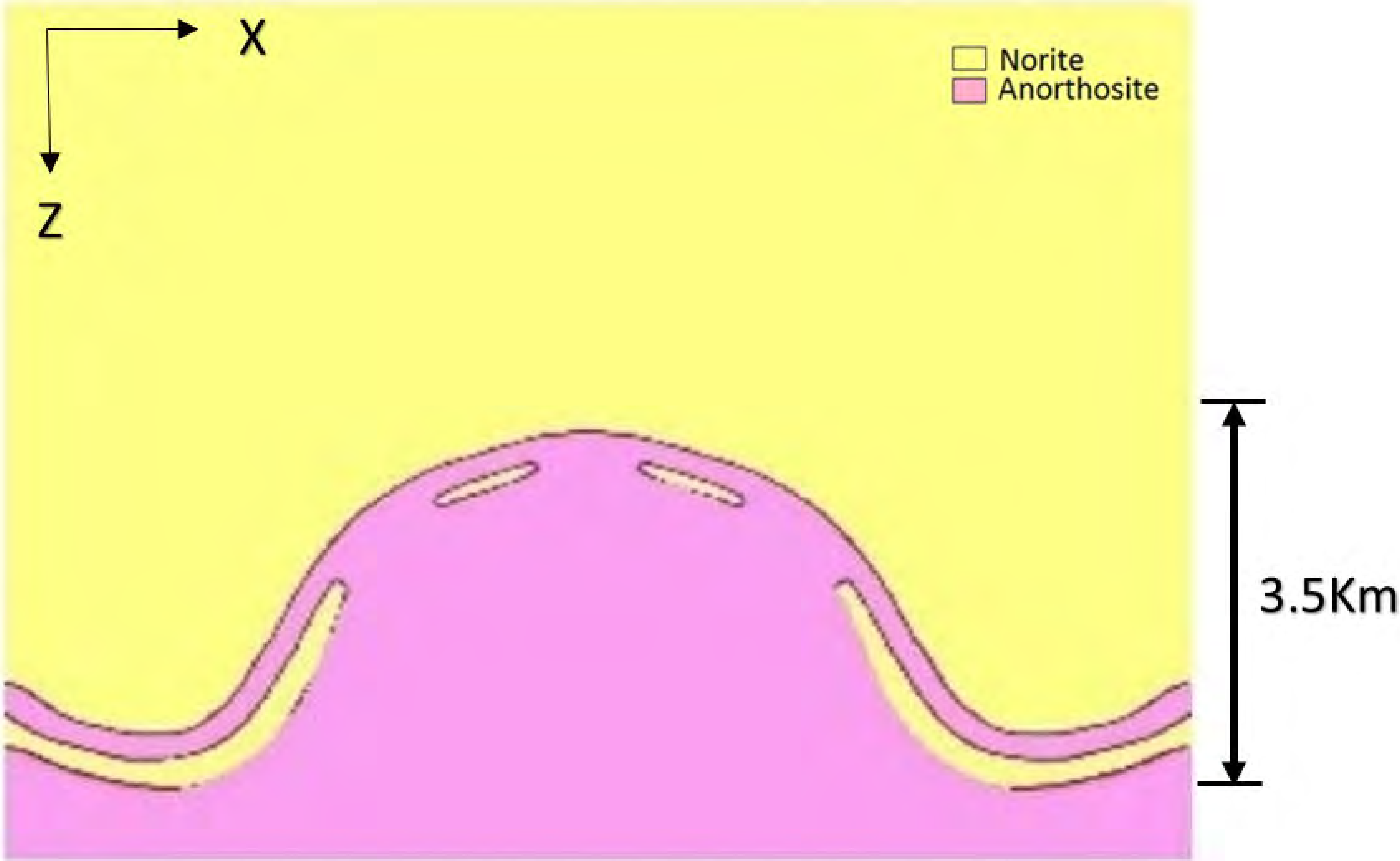
X
Z
Norite
Anorthosite
3.5Km

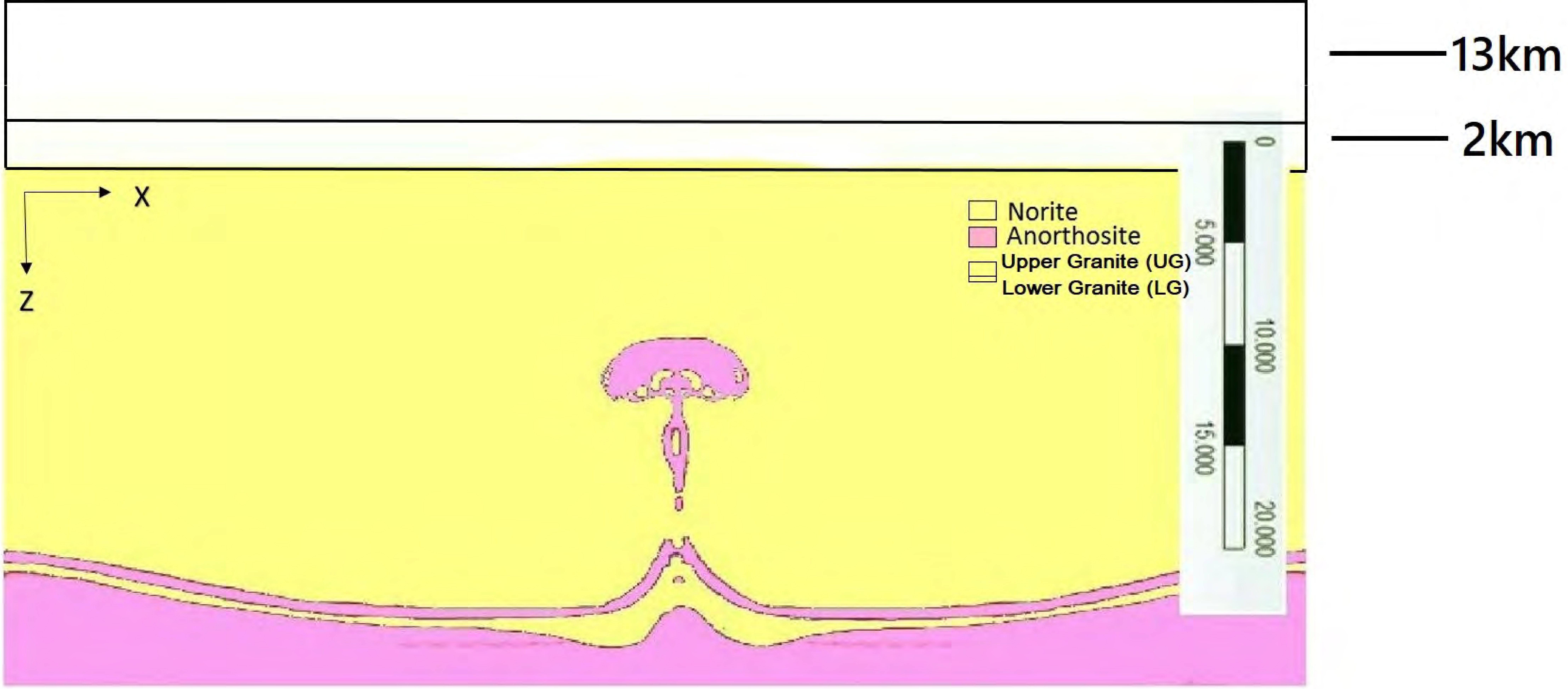
13km
2km
X
Z
Norite
Anorthosite
Upper Granite (UG)
Lower Granite (LG)
0
5.000
10.000
15.000
20.000

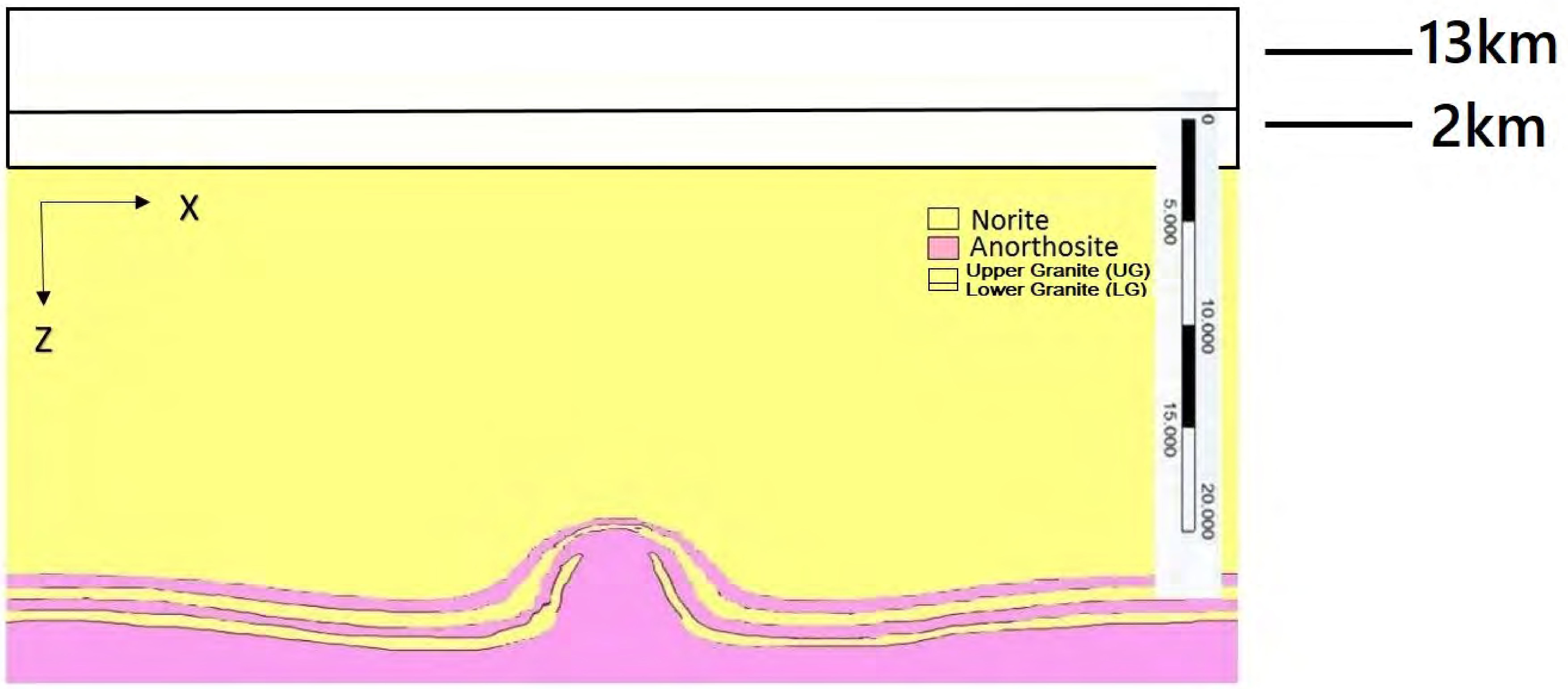
13km
2km
X
Z
Norite
Anorthosite
Upper Granite (UG)
Lower Granite (LG)
0
5.000
10.000
15.000
20.000

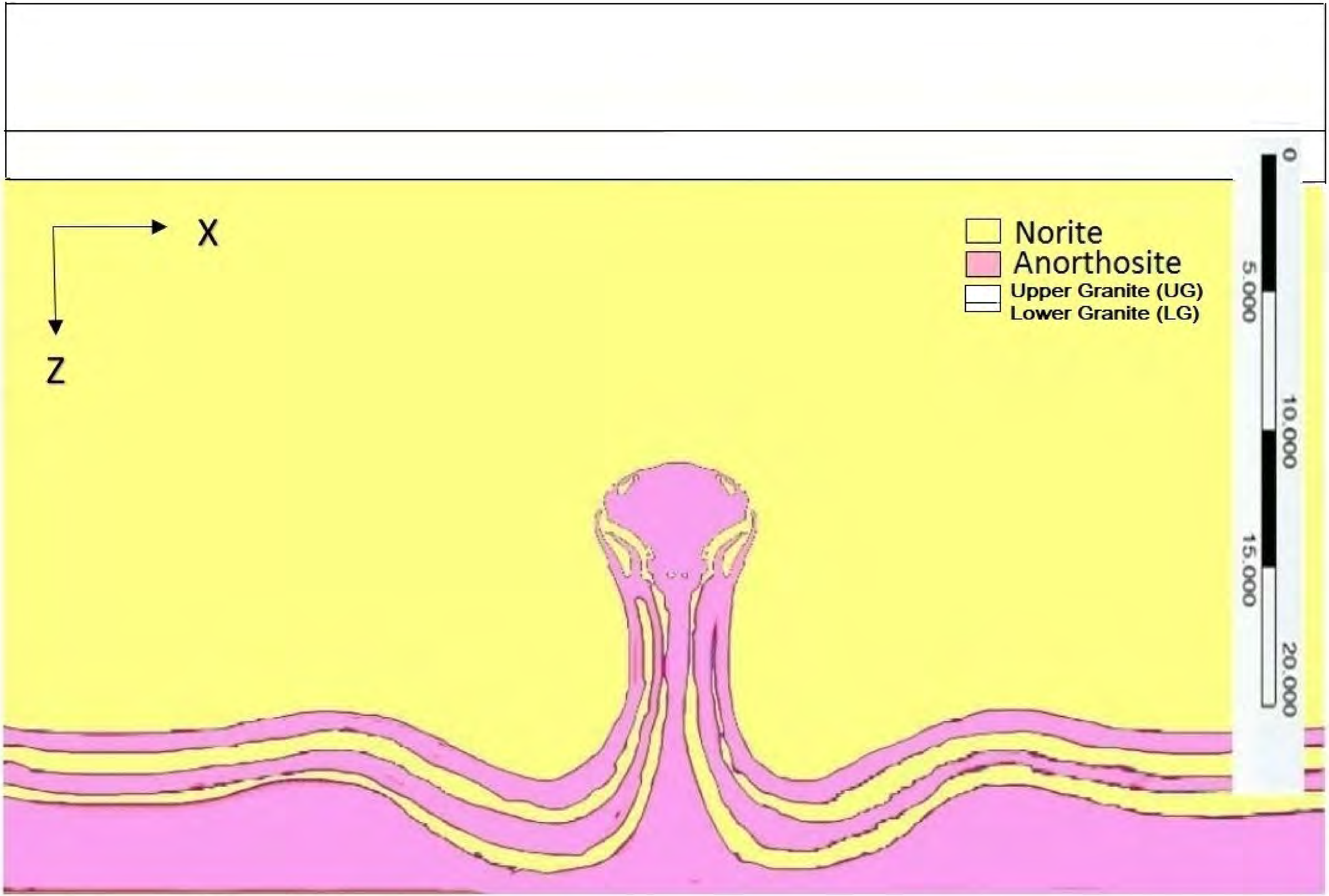
X
Z
Norite
Anorthosite
Upper Granite (UG)
Lower Granite (LG)
0
5.000
10.000
15.000
20.000

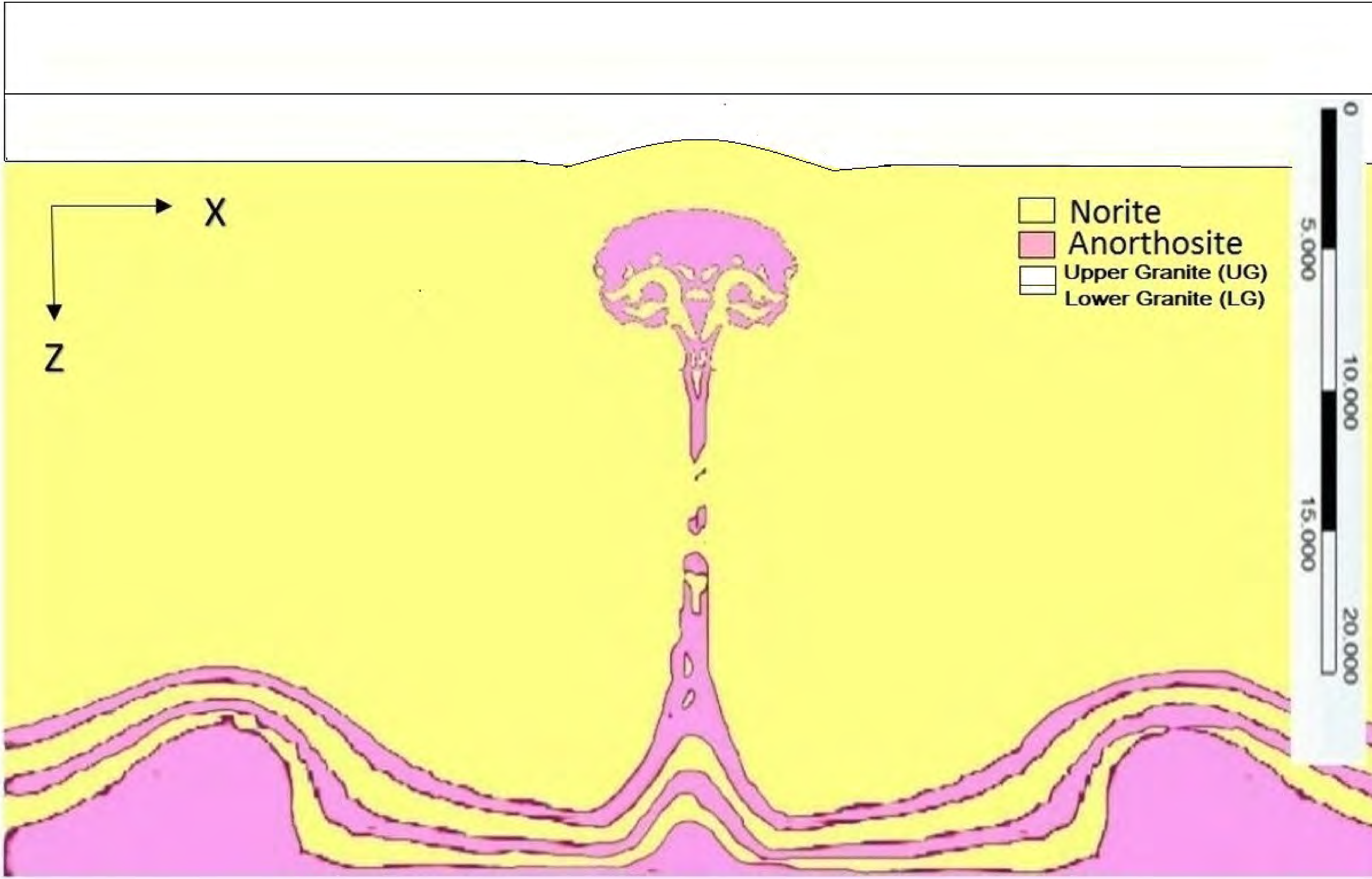
X
Z
Norite
Anorthosite
Upper Granite (UG)
Lower Granite (LG)
0
5.000
10.000
15.000
20.000

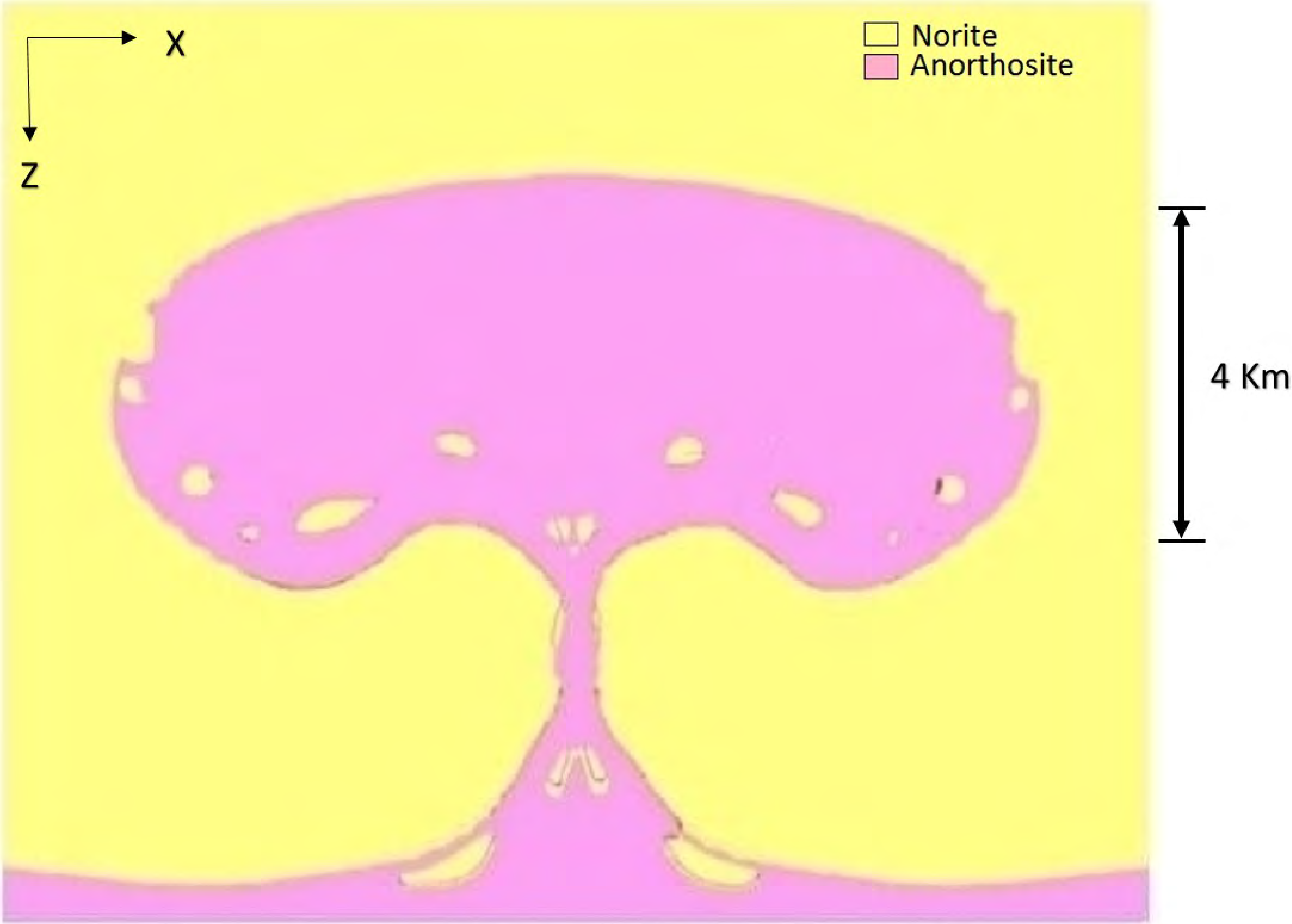
X
Z
Norite
Anorthosite
4 Km

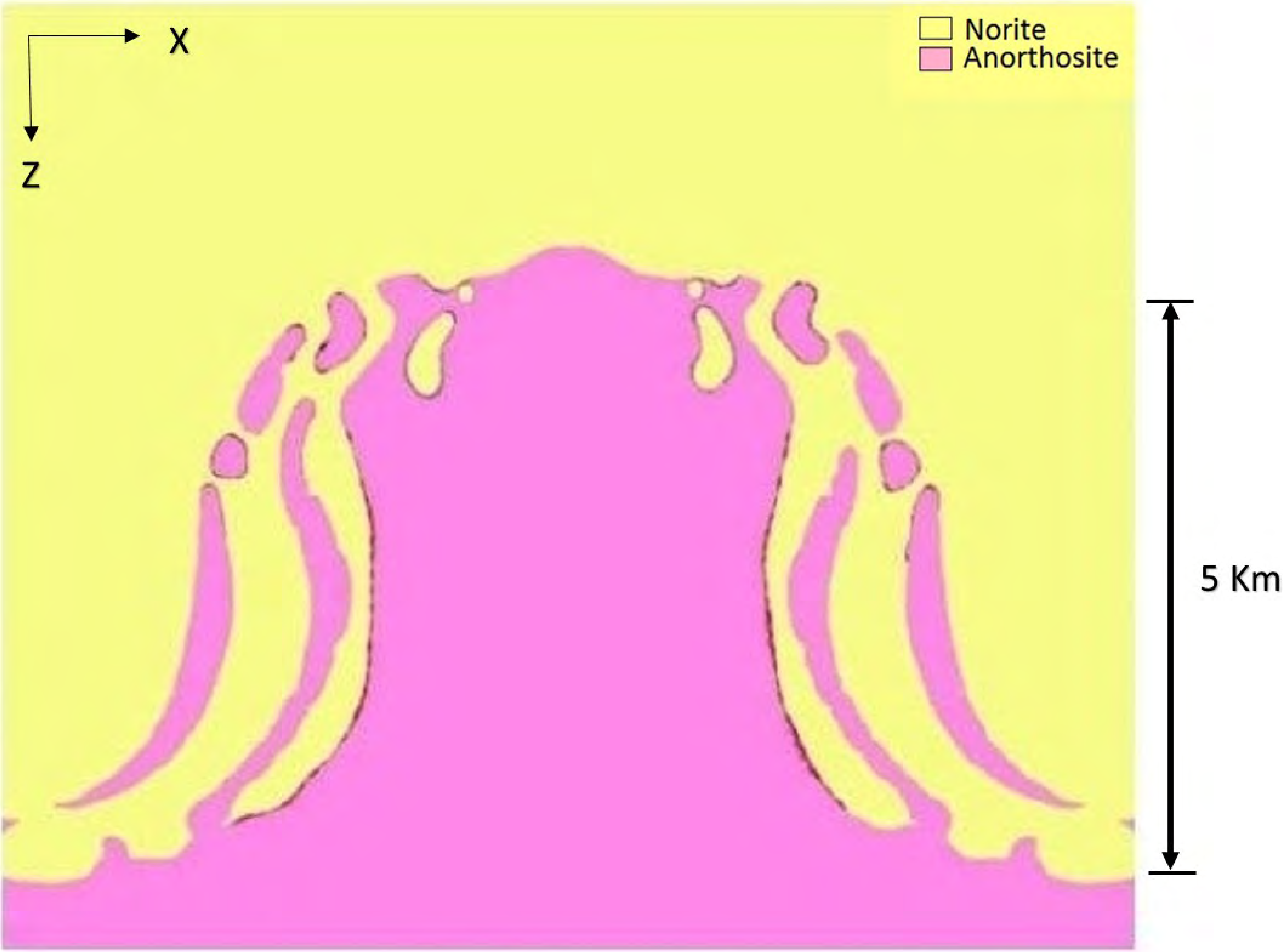
X
Z
Norite
Anorthosite
5 Km